Journal of Theoretical and Applied Information Technology
15th January 2025. Vol.103. No.1

ISSN: 1992-8645 www.jatit.org E-ISSN: 1817-3195

TROPICAL CYCLONE DETECTION IN COASTAL AREA USING RECURRENT ALL-PAIRS FIELD TRANSFORMER FEATURE EXTRACTION AND 3D-CNN CLASSIFICATION MODEL FROM GEOSTATIONARY SATELLITE DATA

NAGU MALOTHU[1,*], DR.V.V.K.D.V.PRASAD[2], DR. B.T.KRISHNA

[1]Researche Scholar, Department of ECE, JNTUK Kakinada, Andhra Pradesh,533003, India.

[2]Supervisor, Professor, Department of ECE, Gudlavalleru Engineering College, Gudlavalleru, Krishna (DT), A.P, 521356, India.

[3]Professor, Department of ECE, UCE JNTUK Kakinada, Andhra Pradesh,533003, India.

E-mail:mng100174@gmail.com

ABSTRACT

High amplitude depending on the wind's top speed and the categorization of intensity are both used in cyclone classification and prediction models. The whole spectrum of ideal features needed for classification are depreciated by the computational limits combined with the production of those intensities, cyclone categorization, and forecast, making accurate representation less likely. There is a bias that varies depending on the Tropical Cyclone (TC) center and shape because there is no standardized way for calculating TC intensity and the most popular method uses a manual computation employing satellite-based weather imagery. The Lucas-Kanade optimal flow based Recurrent All-Pairs Field Transformer (LK RAFT) is thus the main focus of this work for feature extraction. It collects properties at the pixel level, creates 4D comparative quantities at multiple scales for all possible pixel resolutions, and retrieves these values through iteratively notifying a flow field via a recurrent unit. Furthermore, three-dimensional convolutional neural networks (3D-CNN) were used to investigate the correlation between TC intensity and multi-spectral geostationary satellite images. Additionally, we used CNN visualization tool, to examine the properties of multi-spectral satellite-based TC pictures according to intensity. Using images from cyclone samples like OCKHI DEC2017 and VARDAH DEC2016, empirical assessment of the proposed LK RAFT 3DCNN method is carried out with the consideration of variables like accuracy, precision, recall, mean square error and F1-score.

Keywords: *Tropical Cyclone (TC), Prediction, feature extraction, satellite images, optimal flow*

1. INTRODUCTION

Among the most dangerous weather patterns to form beyond a tropical ocean is a tropical cyclone (TC), that has been receiving a significant amount of attention due to its destructive effects on people [1-5]. According to research, the original TC intensity, the meteorological condition of the environment, and the heat exchange in between ocean and TCs all have a significant impact on the density of TC [6-9]. Because of the limited knowledge of TC dynamics and the scarcity of observations over the ocean, it is currently challenging to estimate TC intensity (TCI) with accuracy [10-14].7 More significantly, since the late 1970s, TC has demonstrated a 16–15% worsening tendency over the previous 37 years [15-18], and the present crisis isn't really hopeful. Violent storms, excessive rainfall, storms, earthquakes, as well as other severe catastrophes linked to TCI are endangering human life and property, hence it is crucial to create improved models to better explain and forecast TCI [19-21].

The two main categories of predictive models are arithmetic models and regression techniques. To predict TCI and its course, mathematical results significantly rely on complicated processes. Although cyclone landfall studies aim for good predictive reliability, understanding the environmental factors that affect the cyclone's strength and direction is equally crucial to address this, we will be incorporating a feature extraction method with mutual information (MI) into the forecasting model. This will improve accuracy and provide insight into how the variables governing the changing cyclone system parameters may

interact with one another. Innumerable feature extraction methods, such as pouch and screen methodologies, have been used in multivariate time series analysis to reduce errors while lowering computation cost of predictive modeling. However, the former has a higher computational burden, whereas the latter makes use of statistical techniques that are more effective. It has been demonstrated that MI improves regressive assignment performance when suitable assumptions are made. Given this, the following are the accomplishments of this work:

- As a filter approach for identifying a condensed collection of attributes helpful to our forecasting assignment, we have used Lucas-Kanade optimal flow. It combines with Recurrent All-Pairs Field Transformer, that has demonstrated the power to describe nonlinear timing relationships of a storm. By incorporating intrinsically connected variables particular to the job, their accuracy of the model could be greatly increased.
- Additionally, adopting a three-dimensional convolution neural network (3D-CNN) offers significantly improved performance over traditional recurrent models thanks to its ability to use any recurrent unit as a core component and infinitely larger dilatation and dilated recurring skipping connections.

Here is the outline of the present article: The presentation's second segment, which includes a table, provides a pertinent compilation of studies on cyclone prediction using neural networks. Models for feature extraction and prediction are proposed in Section 3. In section 4, we compare the proposed model's performance to that of a benchmark. In the fifth section, we offer the method's overall conclusion.

2. RELATED WORKS

Additionally, it is undeniable that upper ocean feedback has a substantial impact on TCs; nevertheless, the effectiveness of operational numerical forecast models is severely hindered because so few of these models account for this. Significant improvements in forecast accuracy are necessary because alternative methods, such statistical models, also fail to account for the complex and nonlinear relationship between TC-related parameters. To fix these problems using conventional methods, scientists have been considering using machine learning (ML) to analyze satellite, radar, in-situ data, etc., to make TCs better forecasters in the last year.

Deep convolutional neural network (CNN) models of stimulated tropical cyclone intensity (TCI) were utilized by Xu et al. (2022), as they performed better than the two other previous model (LeNet-5 and AlexNet). The susceptibility studies' findings show strong agreement with the theory and observations, which validates the model's accuracy and dependability. The outcomes also imply that the significance of predictors varies depending on the aim. For accurate, long-lead-time storm surge prediction, Chao et al. (2022) propose a model that combines parametric cyclones with neural networks. The Longdong station region in northern Taiwan was the target of the model's application. Overall, the suggested solution preserved the crucial typhoon indicators while reducing the complexity of the network topology. Specifically, typhoon potential future influence can be inferred utilizing locally-based pressure and wind estimations from storm parameters using physically-based parametric cyclone models, as compared to earlier works' simple collection and direct use of observation data from local stations. Using deep convolutional neural network architecture, Kolukula et al. (2022) adopted a blending method that produces increased wind fields; after the architecture learns the mapping, it can be quickly deployed. Based on two classes of Recurrent Neural Networks (RNNs), which use storm passthrough probabilities calculated from historical data, Bose et al. (2022) proposed their theory. Due to compounded mistake accumulation, a rigorous investigation of model forecasting inaccuracy reveals that Many-To-One prediction models are less accurate than Many-To-Many models. Zhou et al. (2021) set out to develop a new model for a back propagation (BP) neural network that can predict when and how much rain will fall during a typhoon. To identify the model's predictors, we look at how a large number of possible variables interact with the two target variables we listed before. The two modules of the multitask machine learning architecture presented by Wu et al. (2021)—the prediction module and the estimate module—are used to predict the path and strength of tropical cyclones. In their 2019 study, Rüttgers et al. used generative adversarial networks (GAN) with inputs from satellite pictures. Satellite images of historical typhoons that have made landfall on the Korean Peninsula are used to train the neural network. Using the trained GAN, a 6-hour-ahead typhoon track is generated, even though the GAN was not trained for that specific storm. A recurrent neural network is built by Pan et al. in (2019). Its 24-hour prediction error of 5.1 ms is similar to subjective prediction and better than some popular dynamical models.

Experts in meteorology have long voiced their disapproval of machine learning—and deep learning in particular—for what they see as its irrational reliance on data discovery rather than on physical principles to reliably forecast TCs. It's a new challenge to figure out how to make computer attempting to learn forecasting analytics more reliable and the regression technique more credible.

3. SYSTEM MODEL

There are two types of cyclone dataset such as OCKHI_DEC2017 and VARDAH_DEC2016 is chosen, which starts by studying the input satellite image containing the tropical cyclone information. This data is processed using Lucas–Kanade optical flow method for filtering and paring. The paired data is given to Recurrent all pair transformer for optimal frame extraction, which hence find the cyclone patterns. Finally, the extracted feature are given to 3D-CNN. Figure-1 shows the block diagram of cyclone prediction.

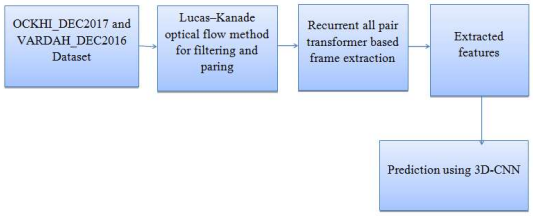

Figure1: Block diagram for cyclone prediction

3.1 Optical flow method

To provide an optical flow approach to address the overall roughness, the Lucas-Kanade optical flow methodology comprises localized limitations [18]. The preceding fractional differential equation is solved using the procedure to provide the optical flow:

$$\frac{\partial J}{\partial u}A + \frac{\partial J}{\partial v}B + \frac{\partial J}{\partial t} = 0 \qquad (1)$$

$I(u, v, t)$ is the lighting of the center pixel on (u, v) at time t., where A and B stand for the flow velocity in the $u$and v directions, correspondingly. Equation (1) (also referred as the optical flow restriction solution, or OFC), incorporates 2 uncontrollable factors that are impossible to solve without an extra condition. The Lucas-Kanade optical flow makes use of the local differentiation approach to determine the pixel's mobility on the presumption that the optical flow is constant in close proximity. As a result, it optimizes the continuity formula for each particular region:

$$\sum G^2(u)[\nabla I(u,t).x + I(u,t)^2 = 0 \qquad (2)$$

where $(A, B)^T$ and $G(u)$ is an effective filter that has a stronger impact on the neighborhood center than the peripheral. The continuity equation (3) can be used to resolve issue (2):

$$M^T G^2 MB = M^T G^2 v \qquad (3)$$

Specifically, $M = [\nabla I(u_1), \dots \nabla I(u_n)]^T$; $v = -\left(I_t(u_1), \dots I_t(u_n)\right)^T$ could be answered by the continuity formula (4)

$$\boldsymbol{B} = [M^T G^2 M]^{-1} M^T G^2 v \qquad (4)$$

Calculations (5) and (6) demonstrate that Calculation (4) is derived in linear system using$M^T G^2 M$is is a nonsingular matrix (6)

$$M^T G^2 M = \begin{pmatrix} \sum G^2(u) I_x^2(x) & \sum G^2(u) I_x(x) y(x) \\ \sum G^2(u) I_x(x) y(x) & \sum G^2(u) \sum G^2(u) I_y^2(x) \end{pmatrix} \qquad (5)$$

$$M^T G^2 v = \begin{pmatrix} G^2 I_x(x) I_t(x) \\ G^2 I_y(x) I_t(x) \end{pmatrix} \qquad (6)$$

Pyramid images at each level are used by the pyramid optical flow to calculate the flow field. The most important step is to build a pyramid with an image sequence, where an elevated shot is converted into a low-resolution view. All calculations should be performed at the subpixel level in order to obtain subpixel accuracy. Table 1 displays the class of Enhanced Fujita scale hurriances.

Table 1: category of Enhanced Fujita scale hurriances scale

EFuj-scale	Class	Speed km/h	Wind mph	description
EFuj-0	Weedy	105-137	65-85	Blow
EFuj-1	Weedy	138-177	86-110	adequate
EFuj-2	Solid	178-217	111-135	substantial
EFuj-3	Solid	218-266	136-165	unembellished
EFuj-4	Intense	267-322	166-200	shattering
EuhF-5	Intense	>322	>200	inconceivable

The steps involved in the subpixel-based LKOF technique are as follows:

- Build a pyramid using two aerial imageries in a cyclical fashion, with level L set to four.
- To acquire motion information in subpixel precision, calculate the subpixel val ue using the bilinear estimation technique among integer values at every level.

Activate the top-level optical flow estimate: $x^{dm} = (A^{dm}, B^{dm}) = (0,0)^T$

Let $d = dm$

- using the conventional Lucas-Kanade procedure Equations (3)–(6) Calculate the residual optical flow $res^L = [res_u^L, res_v^L]$ i at level

- The optical flow $y^{L-1} = (A^{L-1}, B^{L-1})^T$ at level L^{-1} may be calculated using the Equation

$$y^{L-1} = (A^{L-1}, B^{L-1})^T = (2(A^L + d_x^L), 2(B^L + d_y^L)))T$$

- The L-1 layer's image size will be double that of the L layer if the x-or y-axis coefficient equals 2.
- Let L = L – 1, then proceed to step (e) and loop through steps (e) to (f) until L equals zero.
- The optical flow y at level L = 0 (original picture) is finally determined using the formula below.

$$y = (A, B) = (A^0 + d_x^0, B^0 d_Y^0$$

Smoothness constraint: The velocity field must be smoothed since the (A,B) computed in step (h) is noise-sensitive. The Bowler smooth strategy is used to smooth the velocity field (A,B) produced above using the average of the eight closest

3.2 Recurrent All-Pairs Field Transformer based feature extraction

Given two sequential RGB pictures, k_1, k_2 we compute a dense displacement field dis^1, dis^2 that translates each pixel (p, q) in I_2 to its corresponding coordinates $(p', q') = (p + dis^1(p), q + dis^2(q)$ in I_2.

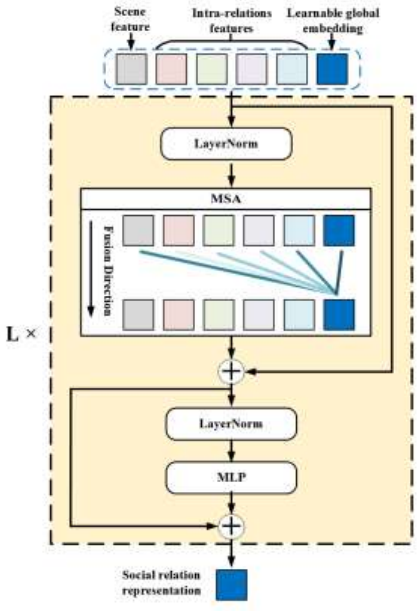

Figure 2: Architecture of Recurrent All-Pairs Field Transformer

Both I1 and I2 use the feature encoder network to convert the input images to lower-resolution dense feature maps. When D is set to 256, our encoder, $g\theta$ outputs feature at a resolution of 1/8, as follows: $g\theta: R^{H\times w\times 3} \rightarrow R^{H/8\times w/8\times D}$. Figure 2 depicts the Recurrent All-Pairs Field Transformer's architectural layout.

Correlation Pyramid: We build a 4-layer pyramid $\{cor^1, cor^2, cor^3, cor^4\}$ by combining the final two main dimensions of the correlation volume with kernel sizes of 1, 2, 4, and 8 with comparable stride. Consequently, the dimensions of the volume cor^k are $H \times W \times \frac{H}{2^k}, \frac{W}{2^k}$. Retaining high resolution information in the first two dimensions (the I_1 dimensions) allows us to recover the movements of small, fast-moving objects, even if the set of volumes exposes both massive and minute displacements. In the first stage of picture cropping, two separate regions and a union region are created utilizing the bounding box information from the labels. The visual indications of a single person, such as their face, attire, and stance, are included in the individual areas, whereas the interaction information between two people is implied by the union region. All of the input data for specialized feature extraction networks is reduced to a consistent 224 × 224 pixels, including the cropped portions and the full pictures used for scene feature extraction. The feature extraction module additionally receives data on the coordinates and areas of two separate bounding boxes, which indicate their relative positions.

Transformer layer: We initially design a feature fusion module called Intra-TRM that is built on transformers. This will allow us to build more realistic social relation representations for each relationship in a picture. As inputs for Intra-TRM, we have both the intra-relation characteristics and the scene attributes from the previous phases. The concept of a transformer design served as the driving force. To facilitate the global fusion of all the retrieved features for each relationship in a single image, we augment the input with an additional global with the same dimension as those features. To globally fuse all the retrieved features for each relationship in a single picture, we append an $extra_{global}$ to the input with the same dimension as those extracted features. The whole input of Intra-TRM (q_{input_intra}) can be expressed as:

$q_{input\_intra)} = [extra_{global}; extra1; extra2; extra3; extra4; extra\ scene], extra_{global}, extra1; extra2; extra3; extra4; extra\ scene \in R^{M\times 2048}$

where $extra1; extra2; extra3; extra4; extra\ scene$ are the features extracted from two individual regions, one union region, relative position and the whole image, correspondingly. When there are N people in a picture, M represents the total number of relationships between them. Then, for more reasonable social relationship representations, we employ a stacking transformer to globally fuse the intra-features and scene characteristics. Additionally, residual connections are created prior to and following each block. The following formula describes the entire process:

$$h'_t = MSA(LN(z_{l-1}))| + z_{l-1}, l = 1,2 \dots L$$
$$h_t = MLP(LN(z'_l)) + z'_l, l = 1,2 \dots L$$

L is set to 12 and represents the number of stacked blocks.

z'_l represents the outputs of the l-th block, whereas z_{l-1} has the same meaning. Standard self-attention extends MSA by executing several self-attention operations (called 'heads') in distinct vector spaces in parallel and concatenating their output for future processing. Layer normalization is denoted by the acronym LN.

3.3 3D-CNN for prediction

Layers three through five of our network's architecture cycle between 3D max pooling and 3D convolutional layers; layers two and three integrate data from the pooled response across the entire input box; and layer five, a Softmax classifier, calculates the class scores and probabilities for each of the twenty cyclone classes.

3D Convolutional Layer: It consists of a set of trainable three-dimensional filters, each of which has a very small input-channel-spanning local receptive field. Over the course of a forward pass, which takes a fixed length of time for each filter, it convolves with its local receptive field at each site to generate filter responses. Similar to the rectified linear (ReLU) activation function, the activation values are determined by sequentially applying a nonlinear change to the filter responses.

When the L_{th} filter is convolved with the input X in, its activation value $ac^L_{i,j,k}$ at output position (i,j,k) may be found using Eqs. (1) and (2).

$$ac^L_{i,j,k} = ReLU[\sum_{m=i}^{i+(Fil-1)} \sum_{n=j}^{j+(Fil-1)} \sum_{d=k}^{k+(Fil-1)} n]$$

$$ReLU = \begin{cases} x, if\ x \geq 0 \\ 0, if\ x < 0 \end{cases}$$

Given the following parameters: X, C, W, F, i, j, k, m, n, and d, where C is the number of input channels, W is a weight matrix with dimensions (C, F, F, F), and the filter size is assumed to be equal in width, height, and depth. Three convolutional neural network architectures are proposed for the use of wind and pressure fields. Since the two types of data need distinct learning rates, we split the networks apart. Since the inputs to the CNNs are several 2D (long, lat) frames or channels, we layered the data across height (pressure level) and time. The Pressure CNN contains six input channels with a size of 25 X 25, but the Wind CNN input has twelve input channels (u and v are layered). Convolutional layers (Conv layer) and max-pooling layers alternated with fully linked layers at the conclusion of a standard CNN design.

4. PERFORMANCE ANALYSIS

The proposed algorithm used satellite images to detect cyclone. The performance of our proposed LK_RAFT_3DCNN is carried out by compared with three state-of-art methods such as VGG-16 [10], Hybrid Neural Network (HNN) [11], deep convolutional neural network architecture (DCNN) [12], Recurrent Neural Networks (RNNs) [13] , back propagation (BP) neural network model [14], multitask machine learning framework (MMLF) [15], generative adversarial network (GAN) [16] .

Dataset description- OCKHI_DEC2017- With OCKHI's evolution, the precipitation fields over the middle Arabian Sea, which experienced extremely heavy rainfall, were affected by dynamical downscaling. The model domain is thus a geographical area measuring approximately 1780 km × 1780 km, bounded by the coastline Arabian Sea between the longitudinal bands of 66°E and 82°E and spanning latitudes 6°N to 22°N. There are 50 vertical levels in all, with the model ceiling set at 10 hPa, the pressure altitude. Each separate simulation was started with the analysis fields corresponding to 00 and 12 UTC of the ICON global model for three days starting from 1 December 2017 to 3 December 2017, and forecast fields for + 48 hours were produced from each of the different simulations.

VARDAH_DEC2016- The cyclone's cloud structure formed in the pre-storm stage, in a region of low pressure, on December 4, 2016, and intensified from December 5 to December 6, 2016, with the duration of the convective clouds increasing the rate of intensification. The increase in intensity from T2.5 to T3 has been detected 24 hours prior to the current observation, as shown by

a tightly curving cloud band that rose by at least 1.50 latitude diameter between 8 and 9 December 2016. After making landfall in the southern coastal areas of Andhra Pradesh and the northern coastal areas of Tamil Nadu, the cyclone's intensity began to weaken after reaching T4 on December 11, 2016.

Experimental results

Table 2: Parametric analysis on OCKHI_DEC2017 dataset

Training data	Accuracy	Precision	Recall	F1-score	MSE
50:60	98.7	87.9	82.4	73.6	12.3
60:70	97.5	88.6	82.1	79.7	11.4
7:80	95.6	86.4	81.6	78.5	15.3
80:90	97.4	87.4	84.5	76.3	11.4
90:100	96.2	83.5	87.3	77.3	16.4
100:110	93.6	86.4	86.3	76.4	14.5

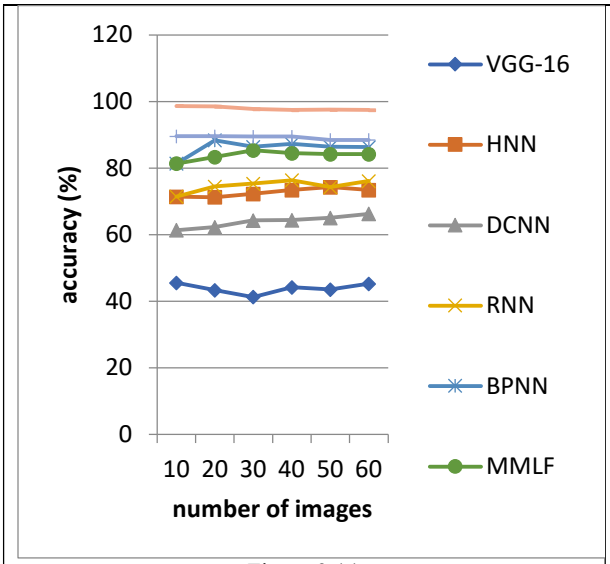

Figure 3 (a)

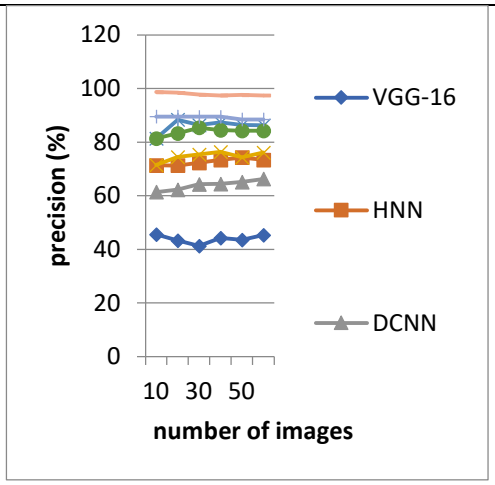

Figure 3 (b)

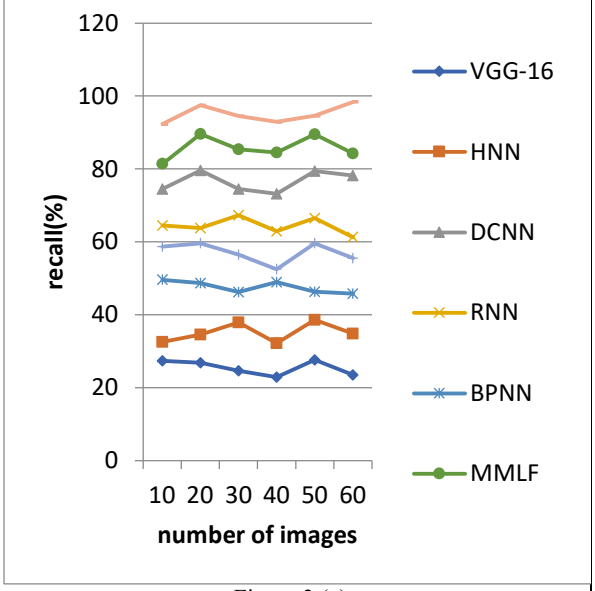

Figure 3 (c)

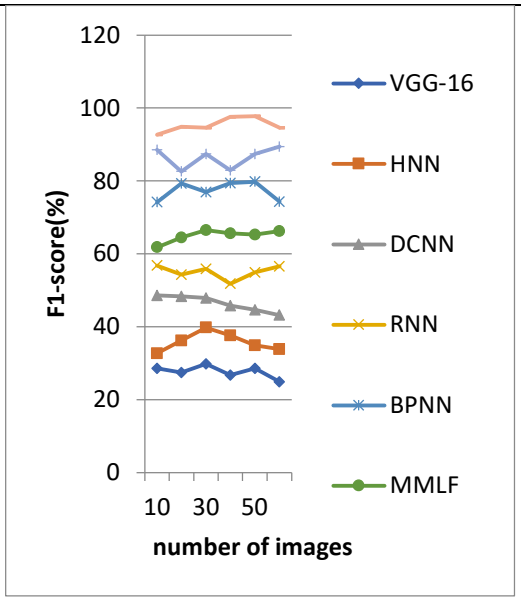

Figure-3 (d)

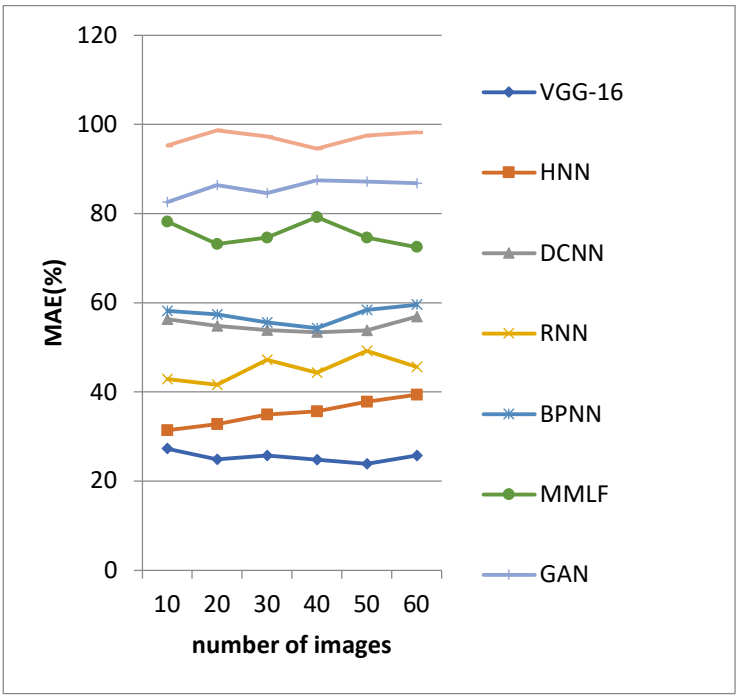

Figure 3 (e)

Figure3: Analysis of various parameters using OCKHI_DEC2017 dataset

Figure 3(a),(b),(c),(d) and (e)(e) indicates the comparison between existing and proposed methods with number of images in x-axis and respective parameters in y-axis for OCKHI_DEC2017 dataset. It is shown that the proposed LK-_RAFT_3DCNN achieves 98.6% of accuracy which is 45.6% better than Vgg-16, 61.4% better than HNN, 45.6% better than DCNN, 32.5% better than RNN, 61.4% better than BPNN, 45.3%better than MMLF, 56.7% better than GAN. In terms of precision the proposed method achieves 89.6% of precision, which is 54.6% better than Vgg-16, 75.4% better than HNN, 23.4% better than DCNN, 32.5% better than RNN, 42.6% better than BPNN, 52.7%better than MMLF, 34.5% better than GAN. In terms of recall the proposed method achieves 84.6% of recall, which is 34.6% better than Vgg-16, 45.3% better than HNN, 62.7% better than DCNN, 45.7% better than RNN, 53.5% better than BPNN, 34.5%better than MMLF, 23.4% better than GAN. In terms of F1-score the proposed method achieves 79.6%, which is 34.6% better than Vgg-16, 65.4% better than HNN, 56.7% better than DCNN, 43.2% better than RNN, 32.6% better than BPNN, 31.4%better than MMLF, 34.6% better than GAN. In terms of MSE the proposed method achieves 15.6%, which is 78.9% lesser than Vgg-16, 89.5% lesser than HNN, 87.5% lesser than DCNN, 78.3% lesser than RNN, 86.5% lesser than BPNN, 84.9%lesser than MMLF, 67.9% lesser than GAN

Table3: Parametric analysis on VARDAH_DEC2016 dataset

Training data	Accuracy	Precision	Recall	F1-score	MSE
50:60	98.6	89.4	81.2	78.9	13.4
60:70	96.5	87.5	81.4	79.5	15.6
7:80	97.6	88.6	84.3	77.8	14.5
80:90	97.5	88.4	83.4	78.9	13.6
90:100	97.5	89.2	83.4	79.7	13.9
100:110	98.5	88.7	85.5	79.4	15.6

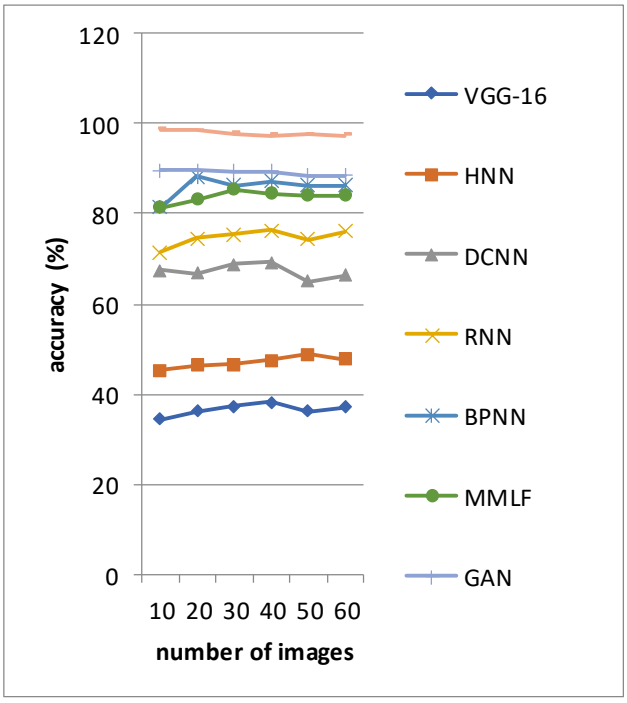

Figure-4 (a)

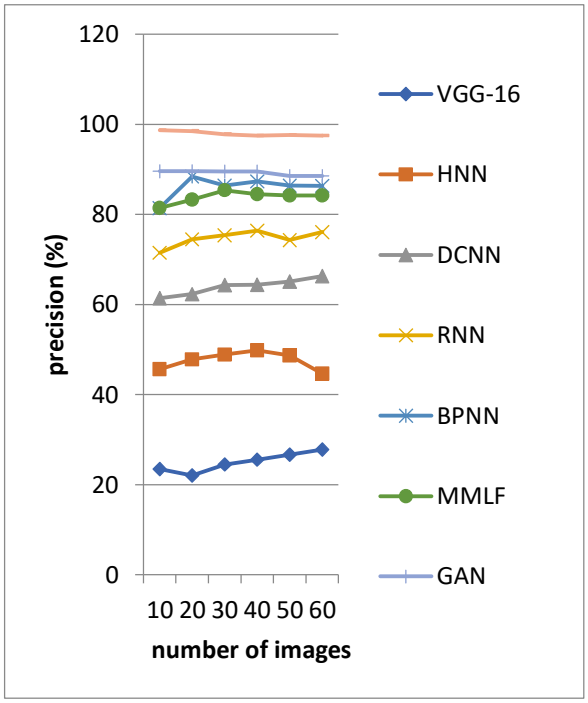

Figure-4 (b)

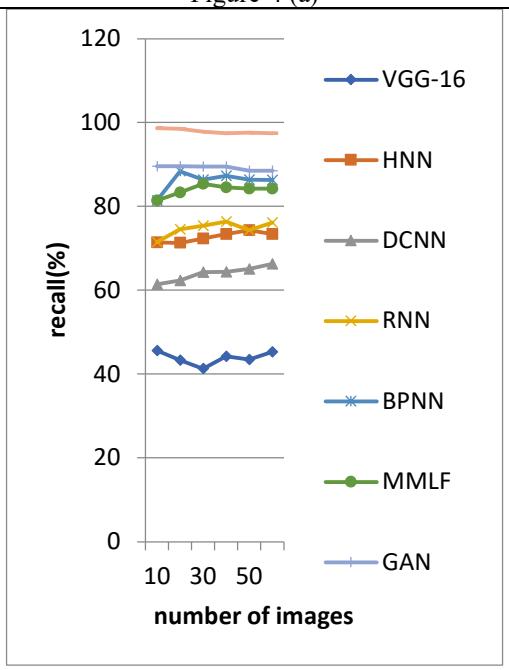

Figure-4 (c)

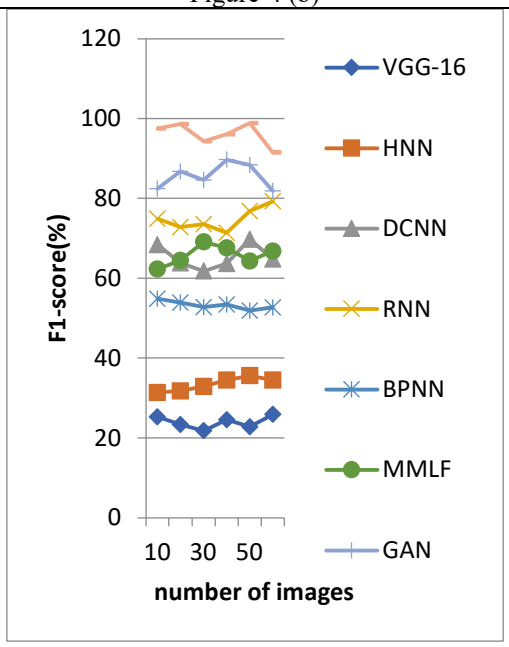

Figure-4 (d)

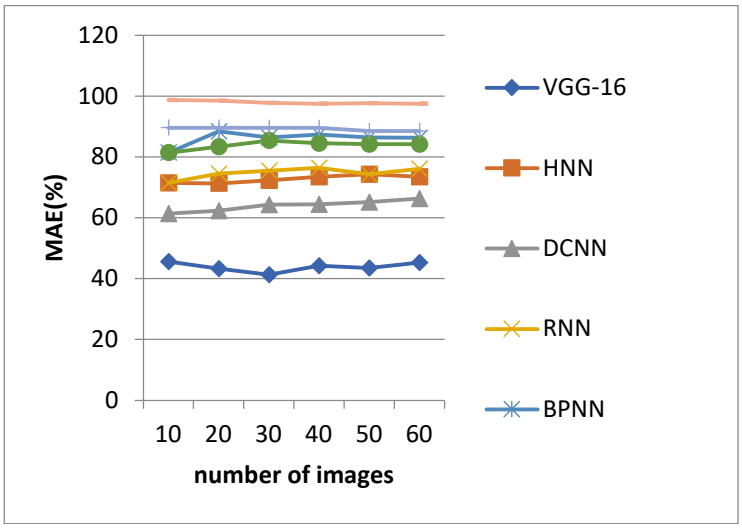

Figure-4 (e)

Figure 4: Analysis of various parameters using VARDAH_DEC2016 dataset

Figure 4(a),(b),(c),(d) and (e) indicates the comparison between existing and proposed methods with number of images in x-axis and respective parameters in y-axis for VARDAH_DEC2016 dataset. It is shown that the proposed LK-_RAFT_3DCNN achieves 98.6% of accuracy which is 34.6% better than Vgg-16, 56.7% better than HNN, 78.9% better than DCNN, 45.8% better than RNN, 78.9% better than BPNN, 56.7%better than MMLF, 46.8% better than GAN. In terms of precision the proposed method achieves 89.6% of precision, which is 54.6% better than Vgg-16, 75.4% better than HNN, 23.4% better than DCNN, 32.5% better than RNN, 42.6% better than BPNN, 52.7%better than MMLF, 34.5% better than GAN. In terms of recall the proposed method achieves 84.6% of recall, which is 56.7% better than Vgg-16, 67.9% better than HNN, 78.5% better than DCNN, 72.6% better than RNN, 45.8% better than BPNN, 34.5%better than MMLF, 23.4% better than GAN. In terms of F1-score the proposed method achieves 79.6%, which is 34.6% better than Vgg-16, 65.4% better than HNN, 56.7% better than DCNN, 43.2% better than RNN, 32.6% better than BPNN, 31.4%better than MMLF, 34.6% better than GAN. In terms of MSE the proposed method achieves 15.6%, which is 78.9% lesser than Vgg-16, 89.5% lesser than HNN, 87.5% lesser than DCNN, 78.3% lesser than RNN, 86.5% lesser than BPNN, 84.9%lesser than MMLF, 67.9% lesser than GAN

5. CONCLUSION

Automated cyclone prediction is continually in demand since they are among the most destructive natural disasters. With the aid of satellite photos and Deep Learning concepts, we have proposed a solution to this significant problem. We have created a two-step feature extraction and classification process to effectively detect cyclones and their core cloud pattern. Although locating a benchmark dataset was a challenge for our completed work, our used technique produced noteworthy results. To expand the scope of our future work, we would like to use more data (such as wind speed, surface temperature, air pressure, etc.) to forecast and track cyclones and to anticipate a more precise center position.

REFERENCES

[1] Srinivasa Sai Abhijit Challapalli. (2024). Sentiment Analysis of the Twitter Dataset for the Prediction of Sentiments. Journal of Sensors, IoT & Health Sciences (JSIHS,ISSN: 2584-2560), 2(4), 1-15. https://doi.org/10.69996/jsihs.2024017.

[2] P. Peduzzi, B. Chatenoux, H. Dao, A. De Bono, C. Herold, J. Kossin, and F. Mouton, O. Nordbeck,"Global trends in tropical cyclone risk", *Nat. Clim. Chang*, Vol.2, pp.289–294,2012.

[3] K.A. Emanuel,"Thermodynamic control of hurricane intensity", *Nature*, Vol.401,pp.665–669,1999.

[4] Y. Xu, L. Zhang, S. Gao, "The Advances and Discussions on China Operational Typhoon Forecasting", *Meteorol. Mon*, Vol.36, pp.43–49,2010.

[5] Srinivasa Sai Abhijit Challapalli, Bala kandukuri, Hari Bandireddi, & Jahnavi Pudi. (2025). Profile Face Recognition and Classification Using Multi-Task Cascaded Convolutional Networks. Journal of Computer Allied Intelligence (JCAI, ISSN: 2584-2676), 2(6), 65-78. https://doi.org/10.69996/jcai.2024029.

[6] W. Mei, S.P. Xie, "Intensification of landfalling typhoons over the northwest Pacific since the late 1970s", *Nat. Geosci.,* Vol.9, pp.753–757,2016.

[7] Y.Chen, P.M. Zhai,"Persistent extreme precipitation events in China during 1951–2010",*Clim. Res.* Vol.57,pp.143–155,2013.

[8] G.J.Van Oldenborgh, K. van der Wiel, A.Sebastian, R. Singh, J. Arrighi, F. Otto, K. Haustein, S.H. Li, G. Vecchi, H. Cullen, "Attribution of extreme rainfall from Hurricane Harvey, August 2017" *Environ. Res. Lett*. Vol.12,pp.124009,2017.

[9] S.N. Jonkman, B. Maaskant, E. Boyd, and M.L. Levitan, "Loss of life caused by the flooding of New Orleans after Hurricane Katrina: Analysis of the relationship between flood characteristics and mortality", *Risk Anal. Off. Publ. Soc. Risk Anal.* Vol.29, pp.676–698,2009.

[10] C.T. Lee, C.C. Huang, J.F. Lee, K.L. Pan, M.L. Lin, and J.J. Dong," Statistical approach to storm event-induced landslides susceptibility" *Nat. Hazards Earth Syst. Sci*.Vol.8,pp.941–960,2008.

[11] X.Y. Xu, M. Shao, P.L.Chen, and Q.G. Wang,"Tropical Cyclone Intensity Prediction Using Deep Convolutional Neural Network" *Atmosphere,* Vol.13,no.5,pp.783,2022.

[12] W.T. Chao, and C.C.Young,"Accurate Storm Surge Prediction with a Parametric Cyclone and Neural Network Hybrid Model" *Water*, Vol.14, No.1,pp.96,2022.

[13] S.S. Kolukula, and P.L.N. Murty,"Improving cyclone wind fields using deep convolutional neural networks and their application in extreme events" Progress in Oceanography, Vol.202, No.102763, 2022.

[14] R. Bose, A. Pintar, and E. Simiu, "A real time prediction methodology for hurricane evolution using LSTM recurrent neural networks", *Neural Computing and Applications*, pp.1-15, 2022.

[15] Y. Zhou, Y. Li, J. Jin, P. Zhou, D. Zhang, S. Ning, and Y.Cui,"Stepwise identification of influencing factors and prediction of typhoon precipitation in Anhui Province based on the Back propagation neural network model" Water, Vol.13, No.4,pp.550, 2021.

[16] Y. Wu, X. Geng, Z. Liu, and Z. Shi, "Tropical cyclone forecast using multitask deep learning framework" I*EEE Geoscience and Remote Sensing Letters*, Vol.19, pp. 1-5,2021.

[17] M. Rüttgers, S. Lee, S. Jeon, and D. You," Prediction of a typhoon track using a generative adversarial network and satellite images", *Scientific reports*, Vol.9, No.1, pp.1-15,2019.

[18] B. Pan, X. Xu, and Z. Shi, " Tropical cyclone intensity prediction based on recurrent neural networks", *Electronics Letters*, Vol. 55, No.7, pp.413-415, 2019.

[19] B.D. Lucas, T. Kanade, "An iterative technique of image registration and its application to stereo", In Proceedings of the 7th International Joint Conference on Artificial intelligence, Vancouver, BC, Canada, 24–28 August 1981; Vol.73, pp. 674–679.

[20] Srinivasa Sai Abhijit Challapalli. (2024). Optimizing Dallas-Fort Worth Bus Transportation System Using Any Logic. Journal of Sensors, IoT & Health Sciences (JSIHS,ISSN: 2584-2560), 2(4), 40-55. https://doi.org/10.69996/jsihs.2024020.

[21] Asmatullah Nashir. (2024). Visual Search Interactive Model for Artificial Intelligence Robotics Model forthe Agricultural Field Analysis. *Journal of Computer Allied Intelligence(JCAI, ISSN: 2584-2676)*, *2*(5), 1-16. https://doi.org/10.69996/jcai.2024021.